

1
2 **Replicative stress in gastroesophageal adenocarcinoma is associated with chromosomal**
3 **instability and sensitivity to DNA damage response inhibitors**

4 Pranshu Sahgal^{1,2,3,8*}, Deepa T. Patil⁴, Zsofia M. Sztupinszki⁵, Viktoria Tisza¹, Sandor Spisak¹, Brandon
5 Huffman¹, Aurel Prosz⁵, Harshabad Singh^{1,2,9}, Jean-Bernard Lazaro^{6,7}, Zoltan Szallasi^{2,5,8}, James M. Cleary^{1,2,9},
6 Nilay S. Sethi^{1,2,3,9,10*}

7
8 ¹ Department of Medical Oncology, Dana-Farber Cancer Institute, Boston, MA, 02215, USA

9 ² Department of Medicine, Brigham and Women's Hospital and Harvard Medical School, Boston, MA, 02115,
10 USA

11 ³ Broad Institute of Massachusetts Institute of Technology (MIT) and Harvard University, Cambridge, MA,
12 02142, USA

13 ⁴ Department of Pathology, Brigham and Women's Hospital, Harvard Medical School, Boston, MA 02215, USA

14 ⁵ Danish Cancer Society Research Center, Copenhagen, 2100, Denmark

15 ⁶ Department of Radiation Oncology, Dana-Farber Cancer Institute, Boston, MA, 02215, USA

16 ⁷ Center for DNA Damage and Repair (CDDR), Dana-Farber Cancer Institute, Boston, MA, 02215, USA

17 ⁸ Computational Health Informatics Program, Boston Children's Hospital, Boston, MA, 02115, USA

18 ⁹ Division of Gastrointestinal Oncology, Department of Medical Oncology, Dana-Farber Cancer Institute, Boston,
19 MA, 02215, USA

20 ¹⁰ Lead Contact

21 *Correspondence:

22 Pranshu Sahgal, Ph.D.

23 Department of Medical Oncology

24 450 Brookline Avenue

25 Dana-Farber Cancer Institute,

26 Boston, MA 02215

27 Phone: 857-269-5957

28 Email: pranshu_sahgal@dfci.harvard.edu

29
30 Nilay S. Sethi, MD, PhD

31 Department of Medical Oncology

32 450 Brookline Avenue, Dana 740

33 Dana-Farber Cancer Institute,

34 Boston, MA 02215

35 Phone: 617-632-3693

36 E-mail: nilay_sethi@dfci.harvard.edu

37

38 SUMMARY

39 Gastroesophageal adenocarcinoma (GEA) is an aggressive, often lethal, malignancy that displays marked
40 chromosomal instability (CIN). To understand adaptive responses that enable CIN, we analyzed paired normal,
41 premalignant, and malignant gastric lesions from human specimens and a carcinogen-induced mouse model,
42 observing activation of replication stress, DNA damage response (DDR), and cell cycle regulator p21 in
43 neoplastic progression. In GEA cell lines, expression of DDR markers correlated with ploidy abnormalities,
44 including high-level focal amplifications and whole-genome duplication (WGD). Moreover, high expression of
45 DNA damage marker *H2AX* correlated with CIN, WGD, and inferior patient survival. By developing and
46 implementing a composite diagnostic score that incorporates *TP53* mutation status, ploidy abnormalities, and
47 *H2AX* expression, among other genomic information, we can identify GEA cell lines with enhanced sensitivity
48 to DDR pathway inhibitors targeting Chk1/2 and Wee1. Anti-tumor properties were further augmented in
49 combination with irinotecan (SN38) but not gemcitabine chemotherapy. These results implicate specific DDR
50 biomarkers and ploidy abnormalities as diagnostic proxy that may predict premalignant progression and response
51 to DDR pathway inhibitors.

53 KEYWORDS

54 Gastric cancer, esophageal cancer, DNA-damage response, aneuploidy, replication stress, CIN, DNA damage
55 response pathway inhibitors, irinotecan

71 INTRODUCTION

72 Gastroesophageal adenocarcinoma (GEA) is a leading cause of death globally and improvement in patient
73 outcomes has been hampered by multiple issues, including failure to identify patients with high-risk precancerous
74 lesions and limited targeted therapy options for patients with advanced disease. The Cancer Genome Atlas
75 project's (TCGA) recent molecular classification has characterized gastroesophageal adenocarcinoma into 4
76 subtypes: microsatellite-unstable, Epstein-Barr virus-positive, chromosomal-instability (CIN), and genomically
77 stable cancers. These classifications have given insight into the molecular features of these subtypes, helping
78 advance the field of early diagnosis and targeted therapies in GEA(Cancer Genome Atlas Research, 2014).

79 The most common GEA subtype is CIN, seen in 50% of patients. The mechanisms leading to and
80 consequences of CIN are still poorly understood(Maleki and Rocken, 2017; Sohn et al., 2017). Nevertheless, CIN
81 is positively correlated with multidrug resistance and ploidy abnormalities, including whole-genome duplication
82 (WGD) and high-level focal amplification events. In addition, recent studies have hypothesized that replicative
83 stress, defined as the presence of stalled replication forks leading to single-strand DNA and possible fork collapse,
84 plays a major role in CIN development. Several proteins in the DNA damage response (DDR) pathway, including
85 Chk1 and Wee1, compensate for replicative stress by slowing the cell cycle and promoting the stability of stalled
86 replication forks(Dominguez-Kelly et al., 2011; Elvers et al., 2012). When these compensatory mechanisms fail,
87 replication forks can collapse and lead to the generation of double-strand DNA breaks, promoting CIN.

88 We hypothesized that high levels of replicative stress are present in GEA CIN oncogenesis. We evaluated
89 the expression of DDR markers in human and mouse gastric precancer and malignant specimens. Further, we
90 assessed whether the GEA cell lines with different levels of DDR and associated ploidy abnormalities correlate
91 with sensitivity to DDR inhibitors in gastric cancer. Recent preclinical and clinical studies suggest that the
92 chemotherapeutic agents that generate replication stress synergize with Chk1 inhibitors across cancers(Banerji et
93 al., 2019). Therefore, we also examined anti-tumor properties of DDR inhibitors in combination with two
94 commonly used chemotherapeutic agents, showing greater therapeutic potential for one pair.

95

96

97 RESULTS

98 Activation of select DDR markers in human gastric premalignancy progression.

99 The progression from premalignancy to cancer is associated with replication stress that leads to DNA double-
100 strand breaks (DSBs) and genomic instability (Macheret and Halazonetis, 2015). To characterize DDR/replication
101 stress in GEA premalignancy progression, we procured human gastric specimens from 8 patients that had matched
102 normal, premalignant, and malignant lesions (Table S1). Using immunohistochemistry (IHC), we evaluated the
103 levels of H2AX/phospho-H2AX (pH2AX) and 53BP1, 2 well-known markers of DNA DSBs and replicative
104 stress (Bartkova et al., 2005; Gupta et al., 2014; Mah et al., 2010). We observed that 53BP1 levels increased during
105 neoplastic progression, with invasive adenocarcinoma displaying the highest levels for nearly all patients (Figure
106 1A-C and Table S2). H2AX and pH2AX were largely absent from normal stomach and premalignant lesions, but
107 malignant lesions from 2 patients showed moderate staining of H2AX and pH2AX (Figure 1A-B, Figure S1A
108 and Table S2). These observations suggest that human gastric premalignant to malignant progression is associated
109 with DNA DSBs and replication stress.

110 Unlike colorectal cancer, GEA harbor early *TP53* mutations, often preceding dysplasia (Sethi et al., 2020;
111 Stachler and Bass, 2020; Stachler et al., 2018; Stachler et al., 2015; Weaver et al., 2014). As GEA evolves, CIN
112 ensues, selecting for amplification of oncogenes and deep deletions of tumor suppressor genes (Liu et al., 2018;
113 Sahgal et al., 2021). We recently showed that *TP53*(p53)/*CDKN2A*(p16) co-altered premalignant gastric
114 organoids derived from a mouse model displayed evidence of early CIN, which was associated with the activation
115 of replication stress and DDR pathways (Sethi et al., 2020). Based on this understanding, we next examined the
116 status of cell cycle regulation markers (p53, p16, and p21) in our samples. We observed marked heterogeneity in
117 p53 and p16 levels among premalignant and malignant lesions, even within a patient. Lesions from the same
118 patient expressed both wild-type (WT) and mutant p53 as well as areas of p16 positivity and negativity (Figure
119 1A). Interestingly, mutant p53 and p16 expression appeared to share an inverse relationship, especially in
120 malignant lesions; p53 WT cells displayed p16 expression whereas p53 mutant cells were p16 negative (Figure
121 1A-C, Figure S1B, and Table S3). A downstream effector of p53, p21 induces cell cycle arrest (Chen, 2016).
122 Notably, we observed a gradual increase in p21 levels in GEA progression; malignant lesions demonstrated
123 significantly higher expression of p21 compared to normal and premalignant lesions in almost all the patients.
124 The glandular, diffuse, and mucinous components of adenocarcinoma showed strong p21 staining, while intestinal
125 metaplasia and dysplasia showed moderate levels (Figure 1A-C, Figure S1B, and Table S3). p21 staining appeared
126 to be independent of mutant p53 expression in gastric cancer progression (Figure 1B-C, Figure S2B, and Table
127 S3). These results indicate that p53 and p16 expression is heterogenous within lesions and through cancer
128 progression, whereas p21 gradually increases from normal to malignant lesions independent of p53 status.

Evaluation of DDR markers in carcinogen-induced mouse model of gastric premalignancy

We next evaluated our panel of biomarkers in a carcinogen-induced (MNU) mouse model of gastric premalignancy and cancer to validate our human observations. Mice exposed to drinking water containing MNU developed premalignant and malignant gastric lesions after 1 to 1.5 years (Sethi et al., 2020). We examined 4 mice treated with MNU that developed varying degrees of dysplasia and cancer (Figure 2A-B), staining formalin-fixed tissue for markers of dsDNA breaks, DDR pathway, and cell cycle regulators. Technical immunostaining limitations precluded interpretation of slides stained for H2AX (dsDNA breaks), 53BP1 (DDR pathway), and p16 (cell cycle). As expected, premalignant and malignant lesions demonstrated greater proliferation compared to normal gastric tissue by Ki67 IHC. We also found the levels of pH2AX, p53, and p16 expression were similar in our mouse lesions compared to the human specimen (Figure 2A-B and S2A); pH2AX was expressed in a premalignant gastric lesion from one mouse and a malignant lesion from another mouse (mouse 3 and 4), but not in normal gastric tissue from any mice. While p53 expression was low in normal gastric tissue, premalignant lesions in mouse 3 and 4 displayed higher p53 expression, consistent with it being mutated. Similarly, p21 was not expressed in normal gastric tissue but was expressed to varying degrees in premalignant and malignant lesions in all 4 mice, with the strongest heterogeneous staining in mouse 3 and 4 (Figure 2A-B and S2A). These results indicate that, like human gastric premalignancy progression, a carcinogen-induced mouse model of gastric adenocarcinoma progression displays increased levels of DDR marker pH2AX and cell cycle regulator p21, with p21 expression independent of p53 mutation status.

Evaluation of DDR markers in TCGA cohort of stomach adenocarcinoma.

To further characterize components of the DDR pathway in human gastric cancer, we evaluated *H2AX* and *TP53BP1* expression in the TCGA stomach adenocarcinoma (STAD) dataset. We observed higher expression of both *H2AX* and *TP53BP1* in gastric adenocarcinoma samples compared with normal gastric tissue (Figures S2B). Interestingly, *H2AX* but not *TP53BP1* expression was significantly higher in *TP53* mutant gastric adenocarcinomas compared to *TP53* WT tumors (Figure S2C). Next, we evaluated the expression of *H2AX* and *TP53BP1* in Lauren's classification subtypes of gastric adenocarcinoma. Lauren's criteria is based on distinct clinical and molecular characteristics that divide gastric adenocarcinoma into intestinal and diffuse subtypes and is the most widely-used histological classification for gastric adenocarcinoma (Lauren, 1965). We observed a significantly higher expression of *H2AX* and not *TP53BP1* in the intestinal subtype than in the diffuse subtype (Figure S2D). Furthermore, *TP53* mutations were more enriched in intestinal subtype patients and in CIN tumors (Figure S2E). These observations suggest the patients with gastric adenocarcinoma that harbor p53 mutations and/or intestinal subtype histology express higher levels of DDR markers such as *H2AX*.

DDR pathway activity is associated with ploidy abnormalities in gastric cancer

164 Since the majority of GEA exhibit ploidy defects as a result of CIN(Maleki and Rocken, 2017), we next
165 evaluated the relationship between CIN and elevated markers of DDR or replication stress. To assess CIN in
166 gastric cancer cell lines, we utilized the CIN25 score(Carter et al., 2006), a gene expression-based validated
167 signature of CIN that predicts clinical outcomes across different human cancers. Indeed, gastric cancer cell lines
168 in the Cancer Cell Line Encyclopedia (CCLE)(Barretina et al., 2012) displayed a strong correlation between the
169 CIN25 score and a recently reported computational metric of aneuploidy (score based on Cohen-Shahir et al.,
170 2021(Cohen-Sharir et al., 2021)) (Figure S3A). Importantly, *H2AX* expression correlated with high CIN25 score
171 in gastric cancer cell lines (Figure 3A). In our analysis, we also found a positive correlation between the
172 aneuploidy score and high-level focal amplifications (Figure S3B), a unique characteristic of gastric cancer
173 evolution(Sahgal et al., 2021), a ploidy score (Figure S3C) and whole genome doubling (WGD) (Figure S3D)
174 (both scores based on Ghandi et al., 2019(Ghandi et al., 2019)). Interestingly, gastric cancer cell lines with WGD
175 have significantly higher expression of *H2AX* compared to ones without WGD (Figure 3B). These analyses
176 suggest that DDR pathway markers, at least *H2AX*, track with WGD and ploidy defects in gastric cancer.

177 To validate the *in silico* analyses, we evaluated five gastric cancer cell lines (AGS, HGC27, HUGC3, GSU,
178 and KE39) that showed varying levels of aneuploidy (Figure 3C) and one non-neoplastic diploid cell line (RPE1).
179 We determined levels of pH2AX and pKAP1 in these cell lines to assess intrinsic DNA DSBs/replication stress.
180 In response to DNA damage and replication stress, KAP1 is phosphorylated at serine 473(White et al., 2006). As
181 expected, RPE1 cells showed minimal staining for pH2AX and pKAP1. Similarly, low levels of pH2AX and
182 pKAP1 were observed in AGS, a TP53 WT gastric cancer cell line displaying the least aneuploidy defects. In
183 contrast, we observed strong and moderate pH2AX and pKAP1 staining in high (KE39 and GSU) and
184 intermediate (HGC27 and NUGC3) aneuploidy cell lines, respectively (Figure 3D). Importantly, since dsDNA
185 breaks correlate with DDR response, these markers tracked with one another. As such, pH2AX and pKAP1 levels
186 positively correlated with the degree of various ploidy defect measurements and p53 mutation status (Figure 3E).
187 GSU and KE39 not only demonstrated greater baseline levels of DNA DSB and replication stress compared to
188 RPE1 and AGS as measured by pH2AX and pKAP1, but also showed a more dramatic, dose-dependent induction
189 when treated with prexasertib(Angius et al., 2020), a well-known Chk1/2 inhibitor (Figure 3F-H). These results
190 demonstrate a correlation between broad measures of ploidy defects and DDR pathway activity in gastric cancer.

191 192 **Gastric cancer with high ploidy abnormalities and high *H2AX* expression are more sensitive to DDR** 193 **pathway inhibitors**

194 Based on these results, we hypothesized that, in addition to the degree of aneuploidy, the level of DDR
195 pathway response to DNA DSBs and replication stress might correlate with sensitivity to drugs that inhibit DNA-
196 damage checkpoint proteins. In other words, the effectiveness of DDR pathway inhibitors for gastric tumors may

depend on levels of DDR activity in the setting of aneuploidy. To test this hypothesis, we used data from the PRISM repurposing drug screen of the BROAD Institute(Corsello et al., 2020) to characterize the sensitivity of the gastric cancer cell lines for DDR pathway inhibitors. Of all the inhibitors examined (Table S4), there was a positive association between higher aneuploidy score and sensitivity to multiple Chk1/2 inhibitors (prexasertib, PF-477736, and Rabusertib) (Figure 4A and Figure S4A). Moreover, higher aneuploidy score and Wee1 inhibitor MK1775 (AZD1775) sensitivity also showed a positive correlation (Figure 4G). Similarly, the CIN25 score in gastric cancer cell lines positively correlated with Chk1/2 inhibitor sensitivity (Figure S4B).

Based on these observations and to further build confidence in our results, we divided the gastric cancer cell lines into 2 groups (quartiles) based on *TP53* status and ‘high or low’ ploidy abnormalities (aneuploidy score, WGD, CIN25 score, high amplitude focal amplifications, and ploidy score). Gastric cancer cell lines with *TP53* mutation and a high degree of ploidy abnormalities were significantly more sensitive to the Chk1/2 (Figure 4B-D) and Wee1 (Figure 4H-J) inhibitors (S4C-G). We also observed that gastric cancer cell lines with specific ploidy defects were sensitive to a subset of ATR inhibitors (AZD6738 for high ploidy cell lines and ETP-46464 for high CIN25 cell lines), but validation experiments using AZD6738 were not able to confirm these results (Figure S4H).

The expression of *H2AX* in gastric cancer cell lines also positively correlated with Chk1/2 inhibitor sensitivity (Figure S4I). Gastric cancer cell lines with high *H2AX* expression were also more sensitive to Chk1/2 and Wee1 inhibitors (Figure 4E, K and S4J). In contrast, gastric cancer cell lines with high ploidy abnormalities were not sensitive to chemotherapeutic agents routinely used in the clinic to treat patients with gastrointestinal cancers. As an example, we show the sensitivity of gastric cancer cell lines with high and low WGD to 8 chemotherapeutic agents (Figure S4K). DDR inhibitors that did not show a significant difference among gastric cancer cell lines with high or low ploidy abnormalities are summarized in Figure S4L-N; there is an enrichment of ATR and ATM inhibitors among these agents.

Encouraged by these results, we validated that gastric cancer cell lines with high ploidy defects (GSU/KE39) showed greater sensitivity to Chk1/2 and Wee1 inhibitors compared to those with low ploidy defects (RPE1/AGS) (Figure 4F, L). These results are in agreement with the correlation plot between aneuploidy and DDR inhibitor sensitivity (Figures 4A and 4G), in which the cell lines used for validation are marked in red. Collectively, these results suggest that biomarkers of DNA DSBs/replication stress and ploidy defects could be predictive markers for DDR pathway inhibitor sensitivity in gastric cancer.

Cumulative score of ploidy abnormalities (CSPA) predicts prexasertib (Chk1/2) response

228 Given the predictive value of individual measures of aneuploidy and DDR pathway activity, we asked
229 whether we could combine these parameters to better predict sensitivity to DDR inhibitors. Indeed, when we
230 combined these parameters using a simple scoring scheme, which we call the cumulative score of ploidy
231 abnormalities (CSPA), we improved the correlation with prexasertib sensitivity ($R^2=0.623$, $P=0.0002$) compared
232 to individual values (*TP53* status, ploidy abnormalities, and *H2AX* expression) (Figure 5A and S5A). Moreover,
233 binning the cell lines into low, medium, and high CSPA yielded a significant difference for prexasertib sensitivity,
234 with high CSPA cell lines showing the greatest prexasertib (Chk1/2 inhibitor) sensitivity (Figure 5B and S5B).
235 As expected, CSPA showed a strong positive correlation with DNA-PKcs (*PRKDC*), a specific marker of DDR
236 activity (Figure S5C). The results from our cumulative score approach suggest that instead of using only one
237 parameter, a combined score, such as CSPA, is a better predictor for DDR inhibitor sensitivity.

238 To understand the relationship between DDR pathway and chemotherapy response in patients with gastric
239 cancer, we decided to examine previously established Recombination Proficiency Score (RPS)(Pitroda et al.,
240 2014) in human gastric cancer gene expression data. RPS can predict adverse clinical features and response to
241 chemotherapy, especially topoisomerase-I inhibiting drugs like topotecan and irinotecan, the latter of which has
242 routinely been used in GEA. Lower RPS depicts inferior patient survival rates, higher genomic stability, and more
243 sensitivity to chemotherapy. In line with our TCGA data analysis, mutant *TP53* gastric cancer in TCGA have
244 lower RPS than wild-type *TP53* patients (Figure S5D), confirming that patients with mutant *TP53* gastric cancer
245 have a poor prognosis and higher sensitivity to irinotecan. Moreover, *H2AX* expression correlates negatively with
246 RPS score in human gastric cancer. Patients with low RPS gastric cancers display higher *H2AX* expression,
247 reinforcing our confidence in *H2AX* expression as a biomarker for tumors exhibiting higher DNA damage and
248 better therapy response (Figure S5E).

249 Chemotherapy is the backbone of most treatment regimens for gastric cancer. We hypothesized that gastric
250 cancers with high DNA DSBs/replication stress would be more sensitive to chemotherapy and DDR pathway
251 inhibitors combination. We therefore sought to identify chemotherapy-DDR pathway inhibitors combinations
252 that enhance cytotoxicity, with the goal of nominating potential clinical trial concepts. KE39 cell line exhibited
253 high DDR pathway activity and therefore a suitable model for these experiments. Based on the recent preclinical
254 and clinical studies, gemcitabine, a chemotherapeutic agent that generates replication stress, showed evidence of
255 synergy when combined with DDR pathway inhibitors in small cell lung cancer, pancreatic cancer, and ovarian
256 cancer(Konstantinopoulos et al., 2020; Sen et al., 2019; Wallez et al., 2018). Irinotecan is also a commonly used
257 chemotherapeutic in the treatment of gastrointestinal cancers. We therefore examined the combination of either
258 gemcitabine or irinotecan with Chk1/2 or Wee1 DDR pathway inhibitors. It is worth noting that while irinotecan
259 is used clinically in gastroesophageal cancer, gemcitabine is not. KE39 cells were generally more sensitive to
260 SN38, the active metabolite of irinotecan(Ramesh et al., 2010) (Figure S5F), than gemcitabine-treated cells.
261 Consistently, SN38 elicited activation of DDR pathway as measured by H2AX, pH2AX, and pDNA-PKcs as well

262 as replication stress as measured by pKAP1 and pRPA32 at lower doses than gemcitabine (Figure 5C and S5G,
263 effect at 1nM for SN38 compared to 10nM for gemcitabine). For the DDR pathway inhibitor prexasertib, the
264 increase in DDR/replication stress marker was first observed at 1nM, with a more substantial increase at 5nM
265 (Figure 5D). When SN38 (2.5nM) was combined with prexasertib or Wee1 inhibitor MK1774 (1.0nM and 5.0nM),
266 the combinations showed a better effect in reducing cell viability and inducing DDR/replication stress compared
267 with the individual monotherapies (Figure 5E-F and Figure S5H). We did not observe this synergy when we
268 combined prexasertib or MK1775 (Wee1) with gemcitabine (Figure S5I).

269 Earlier in this study, we observed an increase in p21 staining during the premalignant to malignant
270 progression in human gastric cancer specimens and in lesions from MNU-treated mice, and found that this
271 staining pattern is independent of p53 status. For SN38 treatment in KE39 cells, the dose-dependent induction in
272 DDR/replication stress correlates with an increase in p21 expression (Figure S5J). This observation is particularly
273 important because KE39 cells harbor a loss-of-function *TP53* mutation. In contrast to the combination with SN38,
274 the combination of gemcitabine with prexasertib or MK1775 was not potent enough to increase DDR/replication
275 stress or p21 levels (Figure S5K). Cumulatively, these clinically relevant data suggest that the combination of
276 irinotecan with Chk1/2 or Wee1 inhibitors is a promising treatment strategy for patients with gastric cancers that
277 display elevated biomarkers of DDR.

278 279 **DISCUSSION**

280 CIN constitutes the largest subtype of gastric cancer, and most of these tumors are heterogeneous, highly
281 aneuploid, and harbor loss-of-function *TP53* mutations (Giam and Rancati, 2015). Replication stress is common
282 cellular stress associated with aneuploidy that results from CIN (Zhu et al., 2018). Moreover, aneuploidy
283 generates replication stress-mediated DNA DSBs, activating the DDR pathway (Ohashi et al., 2015). Failure of
284 cell-cycle control can lead to WGD (Dewhurst et al., 2014; Goyal et al., 2011; Quinton et al., 2021a). Cancer cells
285 with high replication stress are subjected to ploidy abnormalities such greater focal amplifications. As such, CIN
286 gastric cancer is intrinsically challenged by adaptive responses to aneuploidy, such as DDR, which may also
287 reveal unique vulnerabilities that can be exploited for cancer therapy (Quinton et al., 2021b; Zhu et al., 2018).
288 The first part of our study aimed to better understand the contribution of DDR/replication stress in premalignant
289 progression of human gastric cancer.

290 We determined that gastric premalignancy is associated with increased expression of specific DDR markers
291 using matched normal, premalignant, and malignant lesions from 8 patients with gastric cancer and a carcinogen-
292 induced mouse model. The cell cycle markers p53, p16, and p21 showed striking heterogeneity within the same
293 tumor and between the precancerous/cancerous lesions from different samples. For both the patients and mouse
294 model, p21 gradually increased from normal to premalignant to malignant lesions independent of p53 status. p21

is downstream of p53, and its expression independent of p53 has been previously reported in other cancers (Origanti et al., 2013). However, the precise mechanism of how p21 becomes activated in the absence of p53 requires further study. A possible mechanism may be that regulatory feedback systems upregulate p21 in the absence of p53.

Our findings reveal significantly higher expression of DDR markers *H2AX* and *TP53BP1* in stomach adenocarcinomas compared with normal tissue. We also found that higher *H2AX* expression is found in *TP53* mutant gastric cancer, and that *TP53* mutations are predominant in the intestinal and CIN subtype of gastric adenocarcinoma. *H2AX* is a marker of activated DNA damage and has been previously implicated in cancer progression (Bartkova et al., 2005; Krishnan et al., 2020). In addition, we observed that higher expression of *H2AX* correlates with CIN and WGD in gastric cancer. Furthermore, patients with gastric adenocarcinoma that exhibit low RPS indicative of elevated genome instability, adverse clinical features, and enhanced sensitivity to chemotherapy, especially irinotecan, have higher *H2AX* expression. These findings demonstrate that DNA damage and CIN are strongly associated in the evolution of gastric cancer, and that elevated markers of DDR may predict response to treatment.

In line with these results in patients, we found that *TP53* mutation, ploidy abnormalities, and *H2AX* expression independently positively correlate with sensitivity to Chk1/2 and Wee1/2 DDR pathway inhibitors in gastric cancer cell models. The predictive power for DDR pathway sensitivity was improved when these parameters of aneuploidy and DDR were combined. These findings suggest that ploidy abnormalities and *H2AX* expression may have clinical value as biomarkers to predict response to DDR pathway inhibitors (Chk1/2 and Wee1) in patients with gastric and esophageal adenocarcinoma. We further these findings by demonstrating promising data that combining irinotecan with DDR pathway inhibitors improves anti-tumor response in a model of gastric cancer. We hope our study will open new avenues for utilizing DDR markers and ploidy defects as diagnostic proxy that may predict premalignant progression and as an indication for using DDR pathway inhibitors in the treatment of a subset of patients with gastric and esophageal adenocarcinoma.

LIMITATIONS OF THE STUDY

It was challenging to find patient specimen with paired premalignant and malignant lesions. We therefore had limited samples to analyze ($n = 8$), reducing the power of our histopathological analysis. Our in vitro studies were limited to 5 gastric cancer cell lines and one non-neoplastic cell line. Further experimentation in organoids and patient-derived xenografts (PDXs) are warranted to improve preclinical data. We used prexasertib and MK-1775 as potent inhibitors of Chk1/2 and Wee1, respectively, as these DDR inhibitors are commonly used in clinical trials for solid tumors. There are however next-generation DDR inhibitors that may prove less toxic and more efficacious; our results can therefore be used as a proof-of-concept.

329 **AUTHOR CONTRIBUTIONS**

330 Conceptualization: P.S., N.S.S.; Methodology: P.S., D.P., Z.M.S.; Validation: P.S., D.P., Z.M.S.; Formal
331 Analysis: P.S., D.P., Z.M.S.; Investigation: P.S., N.S.S.; Data Curation: P.S., Z.M.S., A.P.; Writing – Original
332 Draft: P.S.; Writing: Review & Editing: P.S., D.P., Z.M.S., V.T., S.S., B.H., A.P., H.S., J-B.Z., Z.S., J.M.C,
333 N.S.S.; Visualization: P.S., D.P., Z.S.; Supervision: Z.S., N.S.S.; Funding Acquisition: P.S., N.S.S.

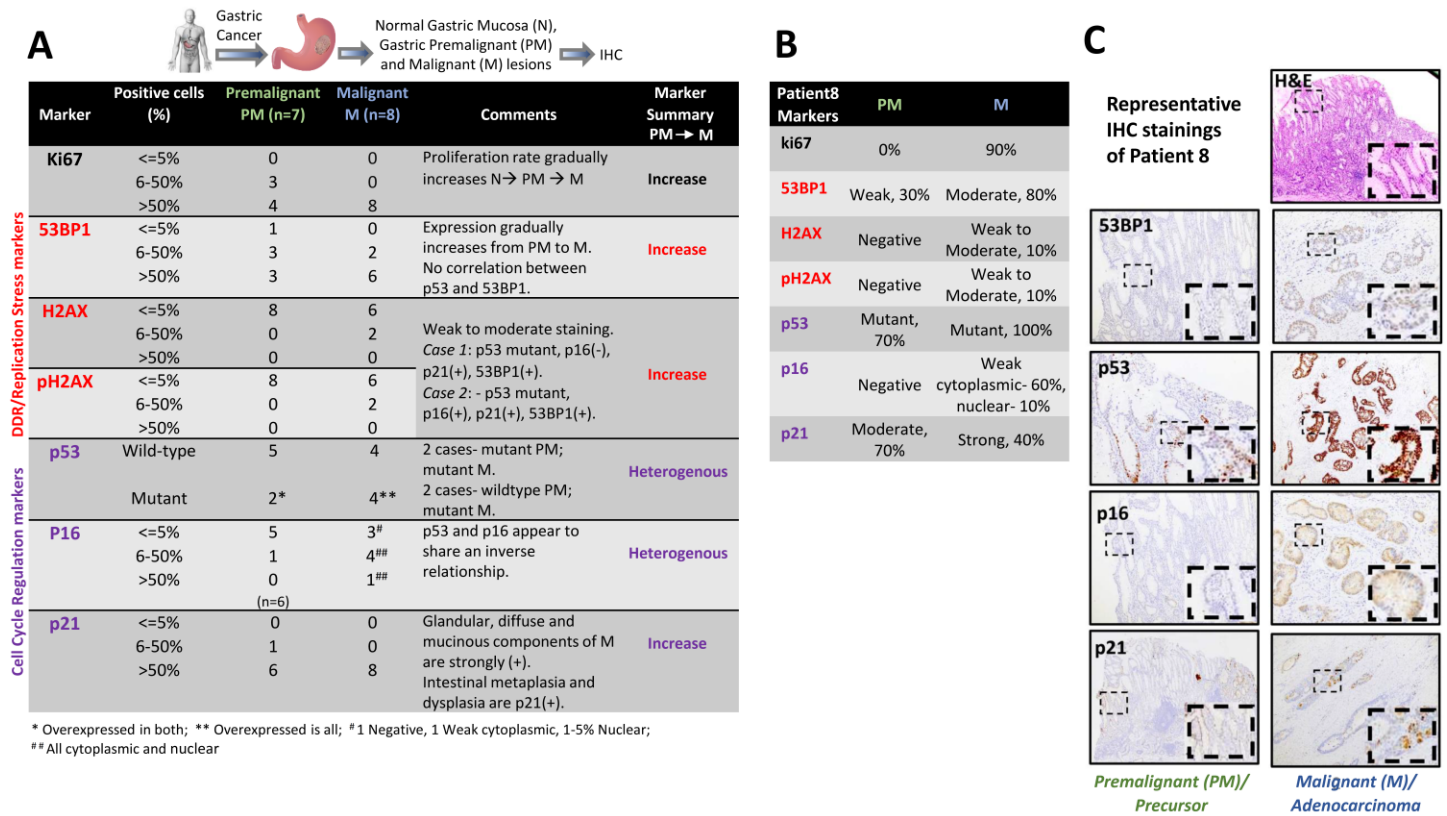
334
335 **ACKNOWLEDGMENTS**

336 The authors thank the pathology core facility of Brigham and Women's Hospital and Beth Israel Deaconess
337 Medical Center for assistance with histopathology; Haley Elizabeth Szewczuga at DFCI for help in editing the
338 manuscript; members of the Sethi lab for insightful discussions. P.S. is Funded by the Finnish cultural foundation
339 and Sigrid Juselius foundation. This study is funded by philanthropic support from Pan-Mass Challenge Team
340 Detect-Me-If-You-Can (Nick Tierney Gastric Cancer Fund) to the Sethi Lab, the National Institute of Health
341 NIDDK K08 (DK120930) (N.S.S), Augustyn Award in Digestive Cancer from the American Gastroenterology
342 Association (N.S.S), Gastric Cancer Foundation (N.S.S), and a DeGregorio Family Foundation Award (N.S.S).

343
344 **DECLARATION OF INTERESTS**

345 N.S.S. is on the advisory board for Astrin Biosciences.
346
347

348 **FIGURE TITLES AND LEGENDS**



* Overexpressed in both; ** Overexpressed is all; # 1 Negative, 1 Weak cytoplasmic, 1-5% Nuclear; ## All cytoplasmic and nuclear

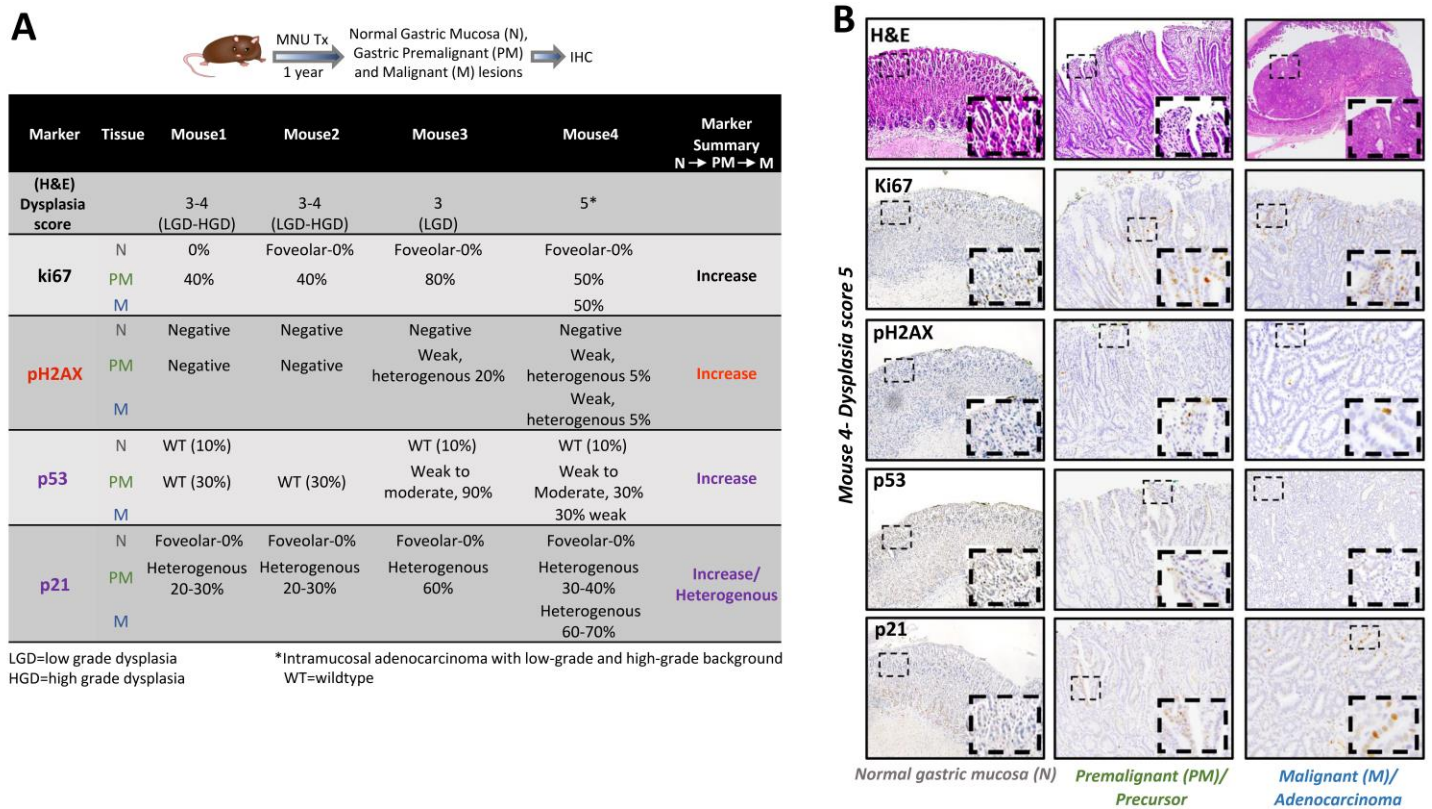
349

350 **Figure 1: Evaluation of DDR and cell cycle markers in human gastric specimens.**

- 351 A. Tabulated summary of IHC stainings indicating the number of premalignant (green) and malignant (blue)
- 352 gastric lesions scored for each staining criterion. DDR/replication stress markers-53BP1, H2AX, pH2AX
- 353 in red; Cell cycle regulators- p53, p16, p21 in purple.
- 354 B. Summary of the stainings (DDR markers and the cell cycle regulation markers) in paired premalignant
- 355 and malignant gastric lesions from gastric cancer patient8. PM= Premalignant gastric lesion, M=
- 356 Malignant gastric lesion.
- 357 C. Representative IHC images of paired premalignant and malignant gastric lesions from a gastric cancer
- 358 patient (patient8) stained for DDR markers and cell cycle regulation markers, including H&E staining.
- 359 Insets represent the zoomed area for each image.

360

361



362
363 **Figure 2: Evaluation of DDR and cell cycle markers in a carcinogen-induced mouse model of gastric**
364 **pre malignancy and cancer**

365 A. Summary of dysplasia grade and staining pattern of proliferation marker ki67, DDR marker pH2AX, and
366 cell cycle regulation markers (p53 and p21) in paired normal (grey), premalignant (green), and malignant
367 (blue) gastric lesions of four MNU treated mice.

368 B. Representative IHC images of the staining pattern of proliferation marker ki67, DDR marker pH2AX, and
369 cell cycle regulation markers (p53 and p21) in paired normal, premalignant, and malignant gastric lesions
370 of MNU treated mouse4 (dysplasia score 5).

371
372

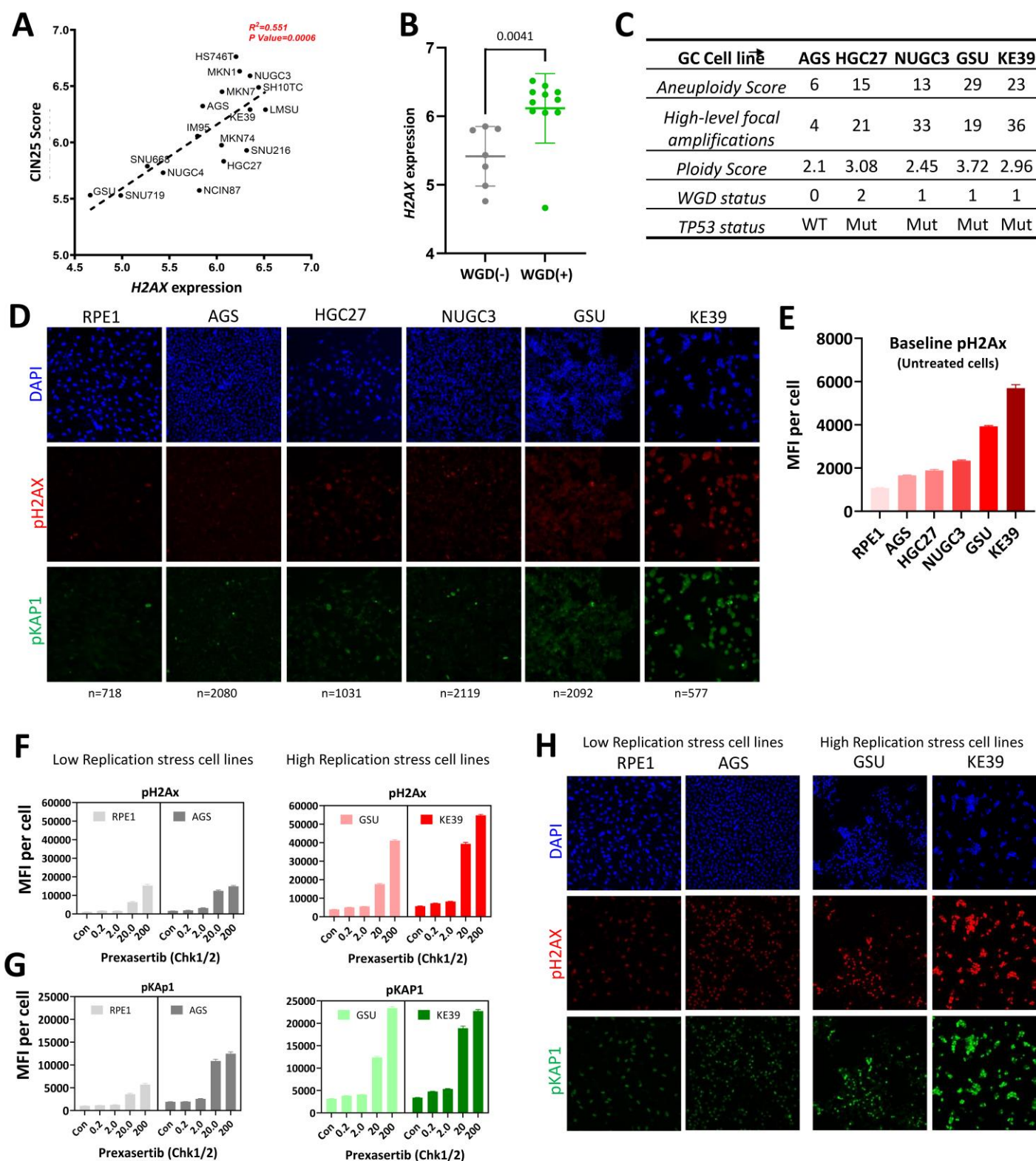


Figure 3: Aneuploidy correlates with DDR, H2AX expression, and replication stress in gastric cancer.

A. Correlation plot between *H2AX* gene expression ($\log_2(\text{TPM}+1)$) and CIN25 score (DNA damage checkpoint expression) for the CCLE gastric cancer cell lines; R squared value and p-value calculated by simple linear correlation analysis.

- 379 B. H2AX expression ($\log_2(\text{TPM}+1)$) between 'No WGD (0)' (grey) and 'with WGD (1/2)' (green) groups of
380 gastric cancer cell lines available in the BROAD institute PRISM repurposing drug screen dataset;
381 Difference between the H2AX expression is represented as the mean \pm S.D.; P-value calculated by unpaired
382 t-test.
- 383 C. Ploidy abnormalities scores for the five gastric cancer cell lines.
- 384 D. Representative immunofluorescence images of pH2AX (red) and pKAP1 (green) stainings in untreated
385 five gastric cancer cell lines and RPE1 cells (non-neoplastic cell line) representing intrinsic replication
386 stress/double-stranded DNA breaks (DSBs); Nucleus stained with DAPI (blue).
- 387 E. Quantification of data in D., expressed as mean fluorescence intensity per cell (MFI) \pm S.D from the
388 following number of cells- RPE1-718, AGS- 2080, HGC27, 1031, NUGC3- 2119, GSU- 2092, KE39-
389 577.
- 390 F. Quantification of pH2AX staining in prexasertib (Chk1/2) dose-dependent induced replication stress in
391 cell lines with 'intrinsic low-replication stress'-RPE1, AGS (grey) and 'intrinsic high-replication stress'-
392 GSU, KE39 (red). Data expressed as mean fluorescence intensity (MFI) of pH2AX signal per cell \pm S.D
393 from the following number of cells- RPE1: Control-718, 0.2nM-888, 2.0nM-524, 20.0nM-570, 200.0nM-
394 350; AGS: Control-2080, 0.2nM-1487, 2.0nM-1996, 20.0nM-1211, 200.0nM- 1396; GSU: Control-2092,
395 0.2nM-3319, 2.0nM-4035, 20.0nM-2057, 200.0nM-2402; KE39: Control-577, 0.2nM-1004, 2.0nM-1022,
396 20.0nM-728, 200.0nM-958.
- 397 G. Quantification of pKAP1 staining in prexasertib (Chk1/2) dose-dependent induced replication stress in
398 cell lines with 'intrinsic low-replication stress'-RPE1, AGS (grey) and 'intrinsic high-replication stress'-
399 GSU, KE39 (green). Data expressed as mean fluorescence intensity of pKAP1 signal per cell \pm S.D from
400 the following number of cells- RPE1: Control-718, 0.2nM-888, 2.0nM-524, 20.0nM-570, 200.0nM- 350;
401 AGS: Control-2080, 0.2nM-1487, 2.0nM-1996, 20.0nM-1211, 200.0nM- 1396; GSU: Control-2092,
402 0.2nM-3319, 2.0nM-4035, 20.0nM-2057, 200.0nM-2402; KE39: Control-577, 0.2nM-1004, 2.0nM-1022,
403 20.0nM-728, 200.0nM-958.
- 404 H. Representative immunofluorescence images of pH2AX (red) and pKAP1 (green) stainings in prexasertib
405 (20nM) treated cell lines with intrinsic 'low-replication stress'-RPE1, AGS, and intrinsic 'high-replication
406 stress'- GSU, KE39.
- 407

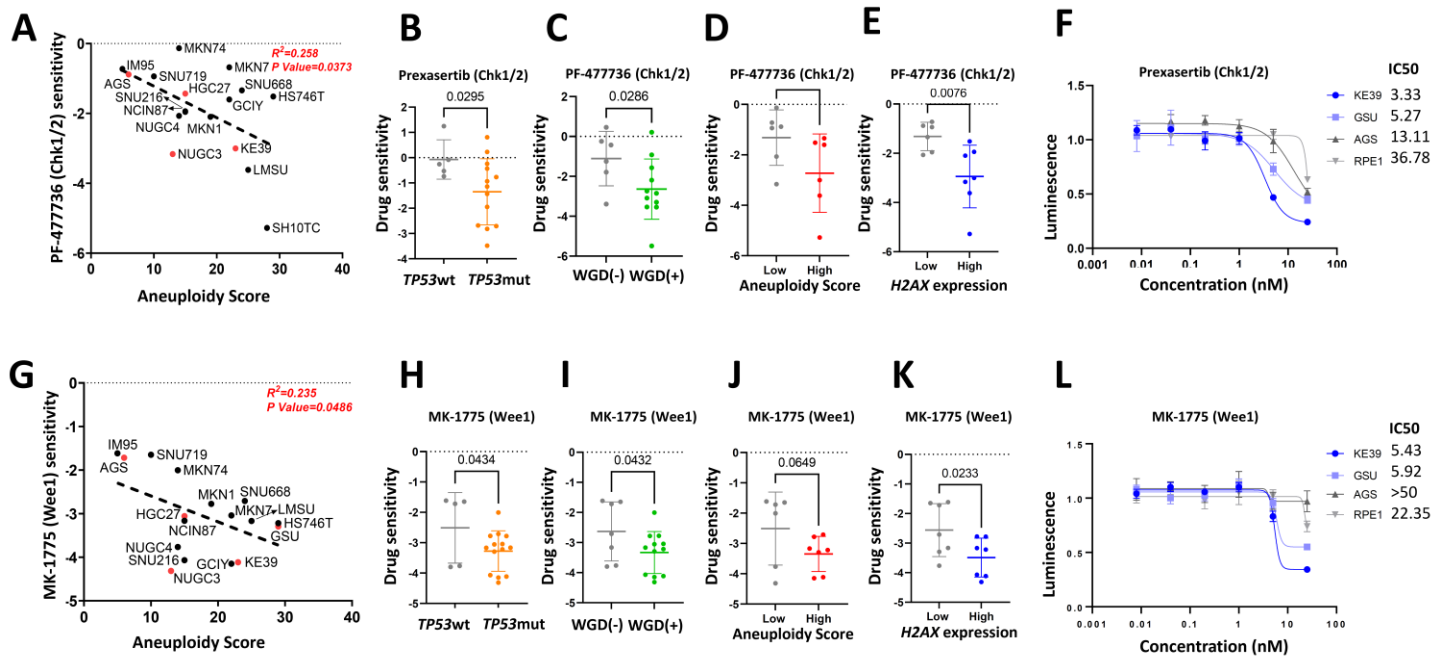


Figure 4: Gastric cancer with high ploidy abnormalities and elevated *H2AX* expression are more sensitive to DDR pathway inhibitors (Chk1/2 and Wee1)

- A. Correlation plot between aneuploidy score and PF-477736 (Chk1/2) sensitivity (log2 fold change) for the CCLC gastric cancer cell lines; Cell lines used in this study marked in red; R squared value and p-value calculated by simple linear correlation analysis.
- B. prexasertib (Chk1/2) sensitivity between 'TP53 wt' and 'TP53 mut' groups of gastric Cancer cell lines BROAD institute PRISM repurposing drug screen dataset; Difference between the prexasertib (Chk1/2) sensitivity (log2 fold change) is represented as the mean±S.D.; P-value calculated by unpaired t-test.
- C. PF-477736 (Chk1/2) sensitivity between 'No WGD (0)' (grey) and 'with WGD (1/2)' (green) groups of gastric cancer cell lines available in BROAD institute PRISM repurposing drug screen dataset; Difference between the PF-477736 (Chk1/2) sensitivity (log2 fold change) is represented as the mean±S.D.; P-value calculated by unpaired t-test.
- D. PF-477736 (Chk1/2) sensitivity between Low aneuploidy score (grey) and high aneuploidy score (red) groups of gastric cancer cell lines available in BROAD institute PRISM repurposing drug screen dataset; Difference between the PF-477736 (Chk1/2) sensitivity (log2 fold change) is represented as the mean±S.D.; P-value calculated by unpaired t-test.
- E. PF-477736 (Chk1/2) sensitivity between 'low *H2AX* expressing' (grey) and 'high *H2AX* expressing' (green) groups (log2(TPM+1)) of gastric cancer cell lines available in BROAD institute PRISM repurposing drug screen dataset; Difference between the PF-477736 (Chk1/2) sensitivity (log2 fold change) is represented as the mean±S.D.; P-value calculated by unpaired t-test.

- 429 F. Dose-response curve of non-neoplastic cell line RPE1, Low replication-stress (grey)-AGS, and high
430 replication-stress (blue)-KE39, GSU gastric cancer cell lines to indicated concentrations of prexasertib
431 (Chk1/2); Best-fit IC50 scores are displayed; Data presented as mean±S.D. of four culture replicates at
432 each indicated dose.
- 433 G. Correlation plot between aneuploidy score and MK-1775 (Wee1) sensitivity (log2 fold change) for the
434 CCLE gastric cancer cell lines; Cell lines used in this study marked in red; R squared value and p-value
435 calculated by simple linear correlation analysis.
- 436 H. MK-1775 (Wee1) sensitivity between 'TP53 wt' and 'TP53 mut' groups of gastric Cancer cell lines
437 BROAD institute PRISM repurposing drug screen dataset; the difference between the MK-1775 (Wee1)
438 sensitivity (log2 fold change) is represented as the mean±S.D.; P-value calculated by unpaired t-test.
- 439 I. MK-1775 (Wee1) sensitivity between 'No WGD (0)' (grey) and 'with WGD (1/2)' (green) groups of gastric
440 cancer cell lines available in BROAD institute PRISM repurposing drug screen dataset; Difference
441 between the MK-1775 (Wee1) sensitivity (log2 fold change) is represented as the mean±S.D.; P-value
442 calculated by unpaired t-test.
- 443 J. MK-1775 (Wee1) sensitivity between low aneuploidy score (grey) and high aneuploidy score (red) groups
444 of gastric cancer cell lines available in BROAD institute PRISM repurposing drug screen dataset;
445 Difference between the MK-1775 (Wee1) sensitivity (log2 fold change) is represented as the mean±S.D.;
446 P-value calculated by unpaired t-test.
- 447 K. MK-1775 (Wee1) sensitivity between 'low H2AX expressing' (grey) and 'high H2AX expressing' (blue)
448 groups (log2(TPM+1)) of gastric cancer cell lines available in BROAD institute PRISM repurposing drug
449 screen dataset; Difference between the MK-1775 (Wee1) sensitivity (log2 fold change) is represented as
450 the mean±S.D.; P-value calculated by unpaired t-test.
- 451 L. Dose-response curve of non-neoplastic cell line RPE1, Low replication-stress (grey)-AGS, and high
452 replication-stress (blue)-KE39, GSU gastric cancer cell lines to indicated concentrations of MK-1775
453 (Wee1); Best-fit IC50 scores are displayed; Data presented as mean±S.D. of four culture replicates at each
454 indicated dose.
- 455
- 456

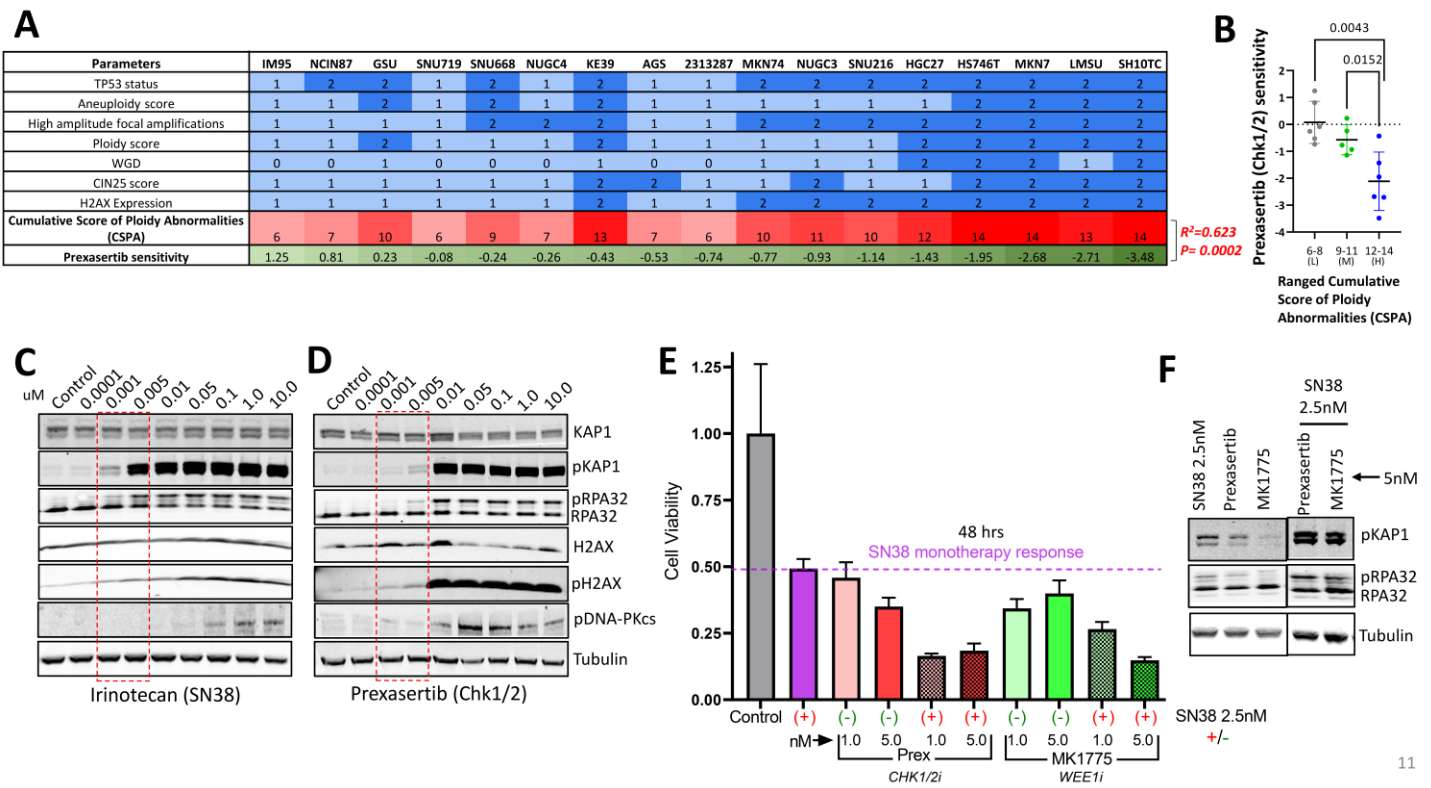


Figure 5: Cumulative score of ploidy abnormalities predicts DDR pathway inhibitor response in gastric cancer cell lines.

- A. Heatmap table representing the correlation between the Cumulative score of ploidy abnormalities and prexasertib sensitivity for the CCLE gastric cancer cell lines. The scoring scheme is as follows: TP53 status: wt=1, mut=2; Aneuploidy score: 15 and less than 15=1, more than 15=2; High amplitude focal amplifications: 20 and less than 20=1, more than 20=2; Ploidy score: 2.5 and less than 2.5=1, more than 2.5=2; WGD: No WGD=0, WGD 1=1, WGD2=2; CIN25 score: 6.1 and less than 6.1=1, more than 6.1=2; H2AX Expression: 6 and less than 6=1, more than 6=2. R squared value and p-value calculated by simple linear correlation analysis.
- B. prexasertib (Chk1/2) sensitivity between three sub-ranged ‘Cumulative score of ploidy abnormalities’ groups of gastric Cancer cell lines BROAD institute PRISM repurposing drug screen dataset; Difference between the prexasertib (Chk1/2) sensitivity (log2 fold change) is represented as the mean±S.D.; L=low, M=medium, H=high; P-value calculated by unpaired t-test.
- C. Immunoblot of replication stress/DDR markers and tubulin as the loading control in the KE39 cell line (high intrinsic replication stress) treated with the indicated concentrations of irinotecan (SN38).
- D. Immunoblot of replication stress/DDR markers and tubulin as the loading control in the KE39 cell line (high intrinsic replication stress) treated with the indicated concentrations of prexasertib (Chk1/2).
- E. Proliferation of the KE39 cell line (high intrinsic replication stress) treated with vehicle (grey), 2.5 nM of SN38 (magenta), prexasertib (red), prexasertib+SN38 (pattered red), MK1775 (green), MK1775+SN38

477 (pattered green); Light shade of color- 1.0nM of DDR inhibitor; Dark shade of color- 5.0nM of DDR
478 inhibitor; All treatments for 48 hrs.

479 F. Immunoblot of pKAP1, pRPA32, and tubulin as the loading control in KE39 cell line (high intrinsic
480 replication stress) treated with monotherapy- SN38 (2.5nm), prexasertib (5nM), MK1775 (5nM) or
481 combination therapy- SN38 (2.5nM)+prexasertib (5nM) and SN38 (2.5nm)+MK1775 (5nM).

482

483

484

485

MATERIALS AND METHODS

Histopathology and Immunohistochemistry

For immunostaining, antigen retrieval was performed using a sodium citrate buffer (pH6), Trilogy (Sigma Aldrich Cell Marque), or Tris-EDTA pH9. Slides were permeabilized using a 0.2% Triton X100 for 30 minutes at room temperature and blocked with donkey serum for 1 hour. The primary antibodies used for immunohistochemistry were: Human tissue- rabbit anti-ki67 (1:1000, Biocare Medical, #CRM325-5b6), rabbit anti-H2AX (1:1000, CST, #7631), rabbit anti-pH2AX ser139 (1:1000, CST, #9718), mouse anti-53BP1 (1:1000, Millipore, #3802), mouse anti-p53 (1:1000, CST, #48818), mouse anti-P16INK4 (1:1000, Abcam, #54210), rabbit anti-p21 (1:1000, CST, #2947), Murine tissue- rabbit anti-ki67 (1:1000, Biocare Medical, #CRM325-5b6), rabbit anti-pH2AX ser139, (1:1000, CST, #9718), rabbit anti-p53 (1:1000, Abcam, #1431), rabbit anti-p21 (1:1000, Abcam, #188224). Binding of primary antibody was detected with 3,3'-diaminobenzidine-tetrahydrochloride-dihydrate and counterstained with hematoxylin. Images were acquired with Leica DM750 microscope. The slides were reviewed by expert GI pathologist (D.T.P.). For each antibody, the percentage positive cells ($\leq 5\%$, 6-50%, and $> 50\%$) were assessed along with intensity of staining (weak, moderate, or strong). For p53, overexpression and null pattern of expression were considered "abnormal" expression while weak, patchy staining was considered normal/wild-type expression. Cytoplasmic and nuclear p16 expression were assessed in all cases.

Cell lines and cell culture

Human gastric cancer cell lines were obtained from the CCLE core facility (BROAD Institute, Cambridge), which obtained them directly from commercial sources and authenticated the lines using standard short tandem repeat analysis. RPE1 cells were obtained from the American Type Culture Collection (ATCC). RPE1 cells were grown in DMEM-F12 (Life Technologies, #10565042) supplemented with 10% FBS and 1% penicillin/streptomycin. HGC27 cells were grown in DMEM (Life Technologies, #11965118) supplemented with 10% FBS and 1% penicillin/streptomycin. AGS, GSU, KE39, and NUGC3 were grown in RPMI 1640 (Life Technologies, #11875119) supplemented with 10% FBS and 1% penicillin/streptomycin. Cells lines were maintained in a humidified 37°C incubator with 5% CO₂ and routinely tested for mycoplasma contamination (Lonza #LT07-118).

Immunofluorescence

Cells were plated on glass-Teflon microscope slide (Tekdon, #518plain) and the next day treated with either DMSO or different concentrations of prexasertib (Selleck, #S7178) for 24 hours. Cells were then washed and fixed with 4% paraformaldehyde (PFA) for 15 minutes at room temperature, blocked and permeabilized PBS-BSA + 0.3% Triton X-100 for 15 minutes at room temperature, and incubated with primary antibodies (rabbit anti-pTIF1 β /pKAP1 (Ser824) (1:500, CST # 4127S) and Mouse anti-pH2AX (1:600, CST #80312) in PBS-BSA

overnight at +4°C. After 3 washes with PBS, secondary antibodies; anti-Rabbit IgG Alexa Fluor 488 (Life tech #A11008) and anti-Mouse IgG Alexa Fluor 568 (Life tech #A11004), diluted 1:300 in PBS-BSA with DAPI (1:1000) for 2 hours at room temperature. Finally, the cells were washed with PBS 3 times, mounted, and covered in aluminum foil for imaging.

Microscopy and Image quantification

Immunofluorescence imaging was performed using Nikon Eclipse Ti2 Series inverted microscope (×40 objective). NIS-Elements AR software was used to acquire the images. DAPI channel was used to focus the cells, and the images for 488 (pKAP1) and 567 (pH2AX) channels were acquired, keeping the same exposure across the samples. For image analysis, the 16-bit images were converted to 2-bit images in ImageJ, followed by 'hole filling' and segmentation (watershed) commands. The cells were then automatically recognized and counted using 'analyze particles', and the file was saved as an 'image mask'. Finally, the image mask was overlaid on the original green (488) and red (567) split channels, and the 'measure' command was used to get the mean fluorescence intensity from each cell.

Cell Proliferation Assay and inhibitors

For IC₅₀ experiments, 1000 cells were plated in a flat-bottom 96-well plate. Cells were treated with either vehicle (DMSO) or different concentrations of the inhibitors. Luminescence was measured using CellTiter-Glo (Promega, #G7572) for ATP amount after 3 days, and final readings were normalized with Day 1 luminescence readings. For colony formation assay, 2x10⁴-1x10⁵ cells were plated in 6-well plates. Cells were then treated with DMSO or inhibitors. After 4-6 days, cells were fixed in 1% paraformaldehyde for 15 minutes at room temperature, washed twice with PBS, and stained with 0.1% crystal violet solution in ethanol (Sigma Aldrich, #HT901) for 15 minutes at room temperature. ImageJ was used to quantify the mean intensity of the scanned plates. The following drug agents were used in the study: prexasertib (Selleck, #S7178), AZD6738 (Selleck, #S7693), MK1775 (Selleck, #S1525), gemcitabine (Selleck, #S1149), and SN-38 (Selleck, #S4908).

Immunoblot

Cells were washed with cold phosphate buffer saline (PBS) and lysed in RIPA buffer (Sigma- Aldrich, #R0278-50ML) supplemented with a protease inhibitor (Roche, #11873580001) and phosphatase inhibitor (CST #5870S). Protein extracts were separated using SDS-PAGE under denaturing conditions (8–16% Novex™ Wedgewell™ Tris-Glycine Gels) and were transferred to PVDF membranes (iBlot2™ PVDF Regular Stacks). Membranes were blocked with blocking buffer (Intercept™ Blocking buffer, #927-60001) and incubated with the primary antibodies diluted in blocking buffer and incubated overnight at +4°C. After primary antibody incubation: rabbit anti-pTIF1β/pKAP1 (Ser824) (1:1000, CST # 4127S), rabbit anti-TIF1β/KAP1 (1:1000, CST

4124S), rabbit anti-H2AX (1:1000, CST #7631), mouse anti-pH2AX (1:1000, CST #80312), rabbit anti- pDNA-PKcs (1:1000, CST, #12311S), rabbit anti- α Tubulin (1:5000, CST, #2125), rabbit anti-p21 (1:500, CST, #2947S), rabbit anti-RPA32 (1:1000, Bethyl, A300-244A) and rabbit anti-pRPA32 (1:1000, Bethyl, A300-246A) membranes were washed 3 times with TBST and incubated with fluorophore-conjugated secondary antibodies diluted (1:10,000) in blocking buffer at room temperature for 1 hour. Membranes were then scanned using an infrared imaging system (Odyssey; LI-COR Biosciences). The following secondary antibodies were used: donkey anti-mouse IRDye 800CW (LI-COR, 926-32212), donkey anti-mouse IRDye 680RD (LI-COR, 926-68072), donkey anti-rabbit IRDye 800CW (LI-COR, 926-32213), and donkey anti-rabbit IRDye 680RD (LI-COR, 926-68073).

TCGA analysis

For the TCGA dataset FPKM-UQ, normalized expression values were downloaded from the TCGA data portal and subtype information was accessed using TCGABiolinks R package(Colaprico et al., 2016). The following subtypes were defined: CIN (chromosomal instability), GS (genomically stable), EBV (Epstein–Barr virus-positive), MSI (microsatellite instability), and HM-SNV (hypermuted-single-nucleotide variant predominant), based on(Liu et al., 2018). World Health Organization (WHO) histological classification was available for these samples and Lauren-classification was determined based on WHO classification. *TP53* mutation status was downloaded from cBioPortal and only pathogenic mutations were treated as mutant cases.

Drug sensitivity and correlation analysis

The gene expression, aneuploidy, and drug sensitivity data were downloaded (22Q2 data release from DepMap website of Broad Institute [<https://depmap.org>]). For the drug sensitivity analysis, the cell lines were divided into a high or low group based on quartiles of the expression of gene of interest, score, or feature. The difference between the mean of sensitivity for the two groups was plotted, and the p-value was calculated using the unpaired t-test. For the correlation analysis, the continuous data were plotted, and R-squared/p-value was calculated using simple linear correlation analysis.

REFERENCES

- Angius, G., Tomao, S., Stati, V., Vici, P., Bianco, V., and Tomao, F. (2020). Prexasertib, a checkpoint kinase inhibitor: from preclinical data to clinical development. *Cancer Chemother Pharmacol* 85, 9-20.
- Banerji, U., Plummer, E.R., Moreno, V., Ang, J.E., Quinton, A., Drew, Y., Hernández, T., Roda, D., Carter, L., Navarro, A., et al. (2019). A phase I/II first-in-human trial of oral SRA737 (a Chk1 inhibitor) given in combination with low-dose gemcitabine in subjects with advanced cancer. *Journal of Clinical Oncology* 37, 3095-3095.
- Barretina, J., Caponigro, G., Stransky, N., Venkatesan, K., Margolin, A.A., Kim, S., Wilson, C.J., Lehar, J., Kryukov, G.V., Sonkin, D., et al. (2012). The Cancer Cell Line Encyclopedia enables predictive modelling of anticancer drug sensitivity. *Nature* 483, 603-607.

- 591 Bartkova, J., Horejsi, Z., Koed, K., Kramer, A., Tort, F., Zieger, K., Guldborg, P., Sehested, M., Nesland, J.M., Lukas, C., *et al.*
592 (2005). DNA damage response as a candidate anti-cancer barrier in early human tumorigenesis. *Nature* *434*, 864-870.
593 Cancer Genome Atlas Research, N. (2014). Comprehensive molecular characterization of gastric adenocarcinoma.
594 *Nature* *513*, 202-209.
- 595 Carter, S.L., Eklund, A.C., Kohane, I.S., Harris, L.N., and Szallasi, Z. (2006). A signature of chromosomal instability inferred
596 from gene expression profiles predicts clinical outcome in multiple human cancers. *Nat Genet* *38*, 1043-1048.
- 597 Chen, J. (2016). The Cell-Cycle Arrest and Apoptotic Functions of p53 in Tumor Initiation and Progression. *Cold Spring*
598 *Harb Perspect Med* *6*, a026104.
- 599 Cohen-Sharir, Y., McFarland, J.M., Abdusamad, M., Marquis, C., Bernhard, S.V., Kazachkova, M., Tang, H., Ippolito, M.R.,
600 Laue, K., Zerbib, J., *et al.* (2021). Aneuploidy renders cancer cells vulnerable to mitotic checkpoint inhibition. *Nature* *590*,
601 486-491.
- 602 Colaprico, A., Silva, T.C., Olsen, C., Garofano, L., Cava, C., Garolini, D., Sabedot, T.S., Malta, T.M., Pagnotta, S.M.,
603 Castiglioni, I., *et al.* (2016). TCGAbiolinks: an R/Bioconductor package for integrative analysis of TCGA data. *Nucleic Acids*
604 *Res* *44*, e71.
- 605 Corsello, S.M., Nagari, R.T., Spangler, R.D., Rossen, J., Kocak, M., Bryan, J.G., Humeidi, R., Peck, D., Wu, X., Tang, A.A., *et*
606 *al.* (2020). Discovering the anti-cancer potential of non-oncology drugs by systematic viability profiling. *Nat Cancer* *1*,
607 235-248.
- 608 Dewhurst, S.M., McGranahan, N., Burrell, R.A., Rowan, A.J., Gronroos, E., Endesfelder, D., Joshi, T., Mouradov, D., Gibbs,
609 P., Ward, R.L., *et al.* (2014). Tolerance of whole-genome doubling propagates chromosomal instability and accelerates
610 cancer genome evolution. *Cancer Discov* *4*, 175-185.
- 611 Dominguez-Kelly, R., Martin, Y., Koundrioukoff, S., Tanenbaum, M.E., Smits, V.A., Medema, R.H., Debatisse, M., and
612 Freire, R. (2011). Wee1 controls genomic stability during replication by regulating the Mus81-Eme1 endonuclease. *J Cell*
613 *Biol* *194*, 567-579.
- 614 Elvers, I., Hagenkort, A., Johansson, F., Djureinovic, T., Lagerqvist, A., Schultz, N., Stoimenov, I., Erixon, K., and Helleday,
615 T. (2012). CHK1 activity is required for continuous replication fork elongation but not stabilization of post-replicative
616 gaps after UV irradiation. *Nucleic Acids Res* *40*, 8440-8448.
- 617 Ghandi, M., Huang, F.W., Jane-Valbuena, J., Kryukov, G.V., Lo, C.C., McDonald, E.R., 3rd, Barretina, J., Gelfand, E.T.,
618 Bielski, C.M., Li, H., *et al.* (2019). Next-generation characterization of the Cancer Cell Line Encyclopedia. *Nature* *569*, 503-
619 508.
- 620 Giam, M., and Rancati, G. (2015). Aneuploidy and chromosomal instability in cancer: a jackpot to chaos. *Cell Div* *10*, 3.
- 621 Goyal, A., Takaine, M., Simanis, V., and Nakano, K. (2011). Dividing the spoils of growth and the cell cycle: The fission
622 yeast as a model for the study of cytokinesis. *Cytoskeleton (Hoboken)* *68*, 69-88.
- 623 Gupta, A., Hunt, C.R., Chakraborty, S., Pandita, R.K., Yordy, J., Ramnarain, D.B., Horikoshi, N., and Pandita, T.K. (2014).
624 Role of 53BP1 in the regulation of DNA double-strand break repair pathway choice. *Radiat Res* *181*, 1-8.
- 625 Konstantinopoulos, P.A., Cheng, S.C., Wahner Hendrickson, A.E., Penson, R.T., Schumer, S.T., Doyle, L.A., Lee, E.K., Kohn,
626 E.C., Duska, L.R., Crispens, M.A., *et al.* (2020). Berzosertib plus gemcitabine versus gemcitabine alone in platinum-
627 resistant high-grade serous ovarian cancer: a multicentre, open-label, randomised, phase 2 trial. *Lancet Oncol* *21*, 957-
628 968.
- 629 Krishnan, V., Lim, D.X.E., Hoang, P.M., Srivastava, S., Matsuo, J., Huang, K.K., Zhu, F., Ho, K.Y., So, J.B.Y., Khor, C., *et al.*
630 (2020). DNA damage signalling as an anti-cancer barrier in gastric intestinal metaplasia. *Gut* *69*, 1738-1749.
- 631 Lauren, P. (1965). The Two Histological Main Types of Gastric Carcinoma: Diffuse and So-Called Intestinal-Type
632 Carcinoma. An Attempt at a Histo-Clinical Classification. *Acta Pathol Microbiol Scand* *64*, 31-49.
- 633 Liu, Y., Sethi, N.S., Hinoue, T., Schneider, B.G., Cherniack, A.D., Sanchez-Vega, F., Seoane, J.A., Farshidfar, F., Bowlby, R.,
634 Islam, M., *et al.* (2018). Comparative Molecular Analysis of Gastrointestinal Adenocarcinomas. *Cancer Cell* *33*, 721-735
635 e728.
- 636 Macheret, M., and Halazonetis, T.D. (2015). DNA replication stress as a hallmark of cancer. *Annu Rev Pathol* *10*, 425-448.
- 637 Mah, L.J., El-Osta, A., and Karagiannis, T.C. (2010). gammaH2AX: a sensitive molecular marker of DNA damage and
638 repair. *Leukemia* *24*, 679-686.
- 639 Maleki, S.S., and Rocken, C. (2017). Chromosomal Instability in Gastric Cancer Biology. *Neoplasia* *19*, 412-420.
- 640 Ohashi, A., Otori, M., Iwai, K., Nakayama, Y., Nambu, T., Morishita, D., Kawamoto, T., Miyamoto, M., Hirayama, T.,
641 Okaniwa, M., *et al.* (2015). Aneuploidy generates proteotoxic stress and DNA damage concurrently with p53-mediated
642 post-mitotic apoptosis in SAC-impaired cells. *Nat Commun* *6*, 7668.

643 Origanti, S., Cai, S.R., Munir, A.Z., White, L.S., and Piwnica-Worms, H. (2013). Synthetic lethality of Chk1 inhibition
644 combined with p53 and/or p21 loss during a DNA damage response in normal and tumor cells. *Oncogene* 32, 577-588.

645 Pitroda, S.P., Pashtan, I.M., Logan, H.L., Budke, B., Darga, T.E., Weichselbaum, R.R., and Connell, P.P. (2014). DNA repair
646 pathway gene expression score correlates with repair proficiency and tumor sensitivity to chemotherapy. *Sci Transl Med*
647 6, 229ra242.

648 Quinton, R.J., DiDomizio, A., Vittoria, M.A., Kotynkova, K., Ticas, C.J., Patel, S., Koga, Y., Vakhshoorzadeh, J., Hermance,
649 N., Kuroda, T.S., *et al.* (2021a). Publisher Correction: Whole-genome doubling confers unique genetic vulnerabilities on
650 tumour cells. *Nature* 593, E15.

651 Quinton, R.J., DiDomizio, A., Vittoria, M.A., Kotynkova, K., Ticas, C.J., Patel, S., Koga, Y., Vakhshoorzadeh, J., Hermance,
652 N., Kuroda, T.S., *et al.* (2021b). Whole-genome doubling confers unique genetic vulnerabilities on tumour cells. *Nature*
653 590, 492-497.

654 Ramesh, M., Ahlawat, P., and Srinivas, N.R. (2010). Irinotecan and its active metabolite, SN-38: review of bioanalytical
655 methods and recent update from clinical pharmacology perspectives. *Biomed Chromatogr* 24, 104-123.

656 Sahgal, P., Huffman, B.M., Patil, D.T., Chatila, W.K., Yaeger, R., Cleary, J.M., and Sethi, N.S. (2021). Early TP53 Alterations
657 Shape Gastric and Esophageal Cancer Development. *Cancers (Basel)* 13.

658 Sen, T., Della Corte, C.M., Milutinovic, S., Cardnell, R.J., Diao, L., Ramkumar, K., Gay, C.M., Stewart, C.A., Fan, Y., Shen, L.,
659 *et al.* (2019). Combination Treatment of the Oral CHK1 Inhibitor, SRA737, and Low-Dose Gemcitabine Enhances the
660 Effect of Programmed Death Ligand 1 Blockade by Modulating the Immune Microenvironment in SCLC. *J Thorac Oncol*
661 14, 2152-2163.

662 Sethi, N.S., Kikuchi, O., Duronio, G.N., Stachler, M.D., McFarland, J.M., Ferrer-Luna, R., Zhang, Y., Bao, C., Bronson, R.,
663 Patil, D., *et al.* (2020). Early TP53 alterations engage environmental exposures to promote gastric premalignancy in an
664 integrative mouse model. *Nat Genet* 52, 219-230.

665 Sohn, B.H., Hwang, J.E., Jang, H.J., Lee, H.S., Oh, S.C., Shim, J.J., Lee, K.W., Kim, E.H., Yim, S.Y., Lee, S.H., *et al.* (2017).
666 Clinical Significance of Four Molecular Subtypes of Gastric Cancer Identified by The Cancer Genome Atlas Project. *Clin*
667 *Cancer Res* 23, 4441-4449.

668 Stachler, M.D., and Bass, A.J. (2020). Can Genomic Sequencing Identify High-Risk Barrett's Esophagus Earlier Than
669 Pathologists? *Cancer cell* 38, 626-628.

670 Stachler, M.D., Camarda, N.D., Deitrick, C., Kim, A., Agoston, A.T., Odze, R.D., Hornick, J.L., Nag, A., Thorner, A.R., Ducar,
671 M., *et al.* (2018). Detection of Mutations in Barrett's Esophagus Before Progression to High-Grade Dysplasia or
672 Adenocarcinoma. *Gastroenterology* 155, 156-167.

673 Stachler, M.D., Taylor-Weiner, A., Peng, S., McKenna, A., Agoston, A.T., Odze, R.D., Davison, J.M., Nason, K.S., Loda, M.,
674 Leshchiner, I., *et al.* (2015). Paired exome analysis of Barrett's esophagus and adenocarcinoma. *Nat Genet* 47, 1047-
675 1055.

676 Wallez, Y., Dunlop, C.R., Johnson, T.I., Koh, S.B., Fornari, C., Yates, J.W.T., Bernaldo de Quiros Fernandez, S., Lau, A.,
677 Richards, F.M., and Jodrell, D.I. (2018). The ATR Inhibitor AZD6738 Synergizes with Gemcitabine In Vitro and In Vivo to
678 Induce Pancreatic Ductal Adenocarcinoma Regression. *Mol Cancer Ther* 17, 1670-1682.

679 Weaver, J.M.J., Ross-Innes, C.S., Shannon, N., Lynch, A.G., Forshew, T., Barbera, M., Murtaza, M., Ong, C.J., Lao-Sirieix,
680 P., Dunning, M.J., *et al.* (2014). Ordering of mutations in preinvasive disease stages of esophageal carcinogenesis. *Nat*
681 *Genet* 46, 837-843.

682 White, D.E., Negorev, D., Peng, H., Ivanov, A.V., Maul, G.G., and Rauscher, F.J., 3rd (2006). KAP1, a novel substrate for
683 PIKK family members, colocalizes with numerous damage response factors at DNA lesions. *Cancer Res* 66, 11594-11599.

684 Zhu, J., Tsai, H.J., Gordon, M.R., and Li, R. (2018). Cellular Stress Associated with Aneuploidy. *Dev Cell* 44, 420-431.

685